Nuclear Inst. and Methods in Physics Research, A 882 (2018) 11–16

Contents lists available at ScienceDirect

Nuclear Inst. and Methods in Physics Research, A

journal homepage: www.elsevier.com/locate/nima

On the resolution of a MIEZE spectrometer

N. Martin

Laboratoire Léon Brillouin, CEA, CNRS, Université Paris-Saclay, CEA Saclay 91191 Gif-sur-Yvette, France

ARTICLE INFO

Keywords:
Neutron spectroscopy
Neutron Spin Echo
Small-angle neutron scattering
MIEZE
Instrumental resolution

ABSTRACT

We study the effect of a finite sample size, beam divergence and detector thickness on the resolution function of a MIEZE spectrometer. We provide a transparent analytical framework which can be used to determine the optimal trade-off between incoming flux and time-resolution for a given experimental configuration. The key result of our approach is that the usual limiting factor of MIEZE spectroscopy, namely neutron path length differences throughout the instrument, can be suppressed up to relatively large momentum transfers by using a proper small-angle (SANS) geometry. Under such configuration, the hitherto accepted limits of MIEZE spectroscopy in terms of time-resolution are pushed upwards by typically an order of magnitude, giving access to most of the topical fields in soft- and hard-condensed matter physics.

A majority of scientific advances are driven by technical development and the topics covered by neutron spectroscopy do not escape this paradigm. Constant efforts aiming at an improvement of momentum (space) or energy (time) resolution are crucial for addressing modern issues in soft- and hard-condensed matter physics. To date, the technique offering the finest energy resolution is Neutron Spin Echo (NSE) spectroscopy which allows studying slow processes (*i.e.* with characteristic times approaching the μs range), provided that the carefully manipulated beam polarization is not degraded by the sample or its environment [1]. Here we consider a derivative of NSE, the so-called MIEZE technique, where all spin manipulations are performed upstream of the sample position. At equivalent technical resolution, MIEZE is potentially more versatile than NSE since it works with any kind of samples (*e.g.* hydrogen-containing systems [2], multi-domain ferromagnets [3], *etc.*) and under extreme conditions (*e.g.* large magnetic fields [4]). On the downside, being a time-of-flight technique, the efficiency of the method is limited towards high resolution by deviations from the optimal neutron flight path across the setup. Here, we show that these limitations can be drastically softened by using MIEZE in a small-angle (SANS) configuration. Our findings clearly pledge for the construction of a dedicated MIEZE-SANS instrument. Its performances can be quantified using the analytical framework developed in this paper.

1. Principles and limits of MIEZE spectroscopy

In the late eighties, R. Golub and R. Gähler have proposed an alternative design to solenoid-based NSE spectrometers, relying on the use of compact radio-frequency spin flippers (RFSF) and hence termed Neutron Resonance Spin Echo (NRSE) [6]. NRSE is now available at different instruments throughout the world (MUSES [7] at LLB-Saclay and IN22-ZETA [8] at ILL-Grenoble in France, RESEDA [9] and TRISP [10] at MLZ-Garching, V2-FLEXX [11] at BER II-Berlin in Germany, VIN ROSE [12] at J-PARC/MLF in Japan) and has opened new experimental perspectives by pushing the usual resolution limits of inelastic scattering [13–15] and diffraction [16,17]. As noticed in the early stages of the development of NRSE, series of resonant neutron spin flips can used as building blocks for alternative spectroscopic methods, in analogy with pulse sequences employed in nuclear magnetic resonance (NMR). MIEZE is an elegant application of this idea [18]. A sketch of a typical MIEZE setup is shown in Fig. 1. It consists in a pair of RFSFs separated by a distance L_1 and operated at angular frequencies ω_1 and $\omega_2 \neq \omega_1$, respectively. At a distance L_2 downstream of the second RFSF, where we choose to place a time-resolved detector, the spin phase of a neutron reads [19]

$$\varphi_D = \omega_M \cdot t_D + \frac{2}{v} \cdot \left[\omega_2 L_1 - \frac{\omega_M}{2} \cdot \left(L_1 + \underbrace{L_{2S} + L_{SD}}_{L_2} \right) \right] \quad , \tag{1}$$

where $\omega_M = 2(\omega_2 - \omega_1)$ is the modulation (or MIEZE) angular frequency, t_D the absolute detection time, v the neutron velocity, L_{2S} the distance between the second flipper and the sample and L_{SD} the sample-to-detector distance. The velocity-dependent part of Eq. (1) is canceled by fulfilling the focusing condition

$$\omega_M = 2\omega_2 \cdot \frac{L_1}{L_1 + L_{2S} + L_{SD}} \quad , \tag{2}$$

E-mail address: nicolas.martin@cea.fr.

https://doi.org/10.1016/j.nima.2017.11.021
Received 9 October 2017; Accepted 7 November 2017
Available online 11 November 2017
0168-9002/

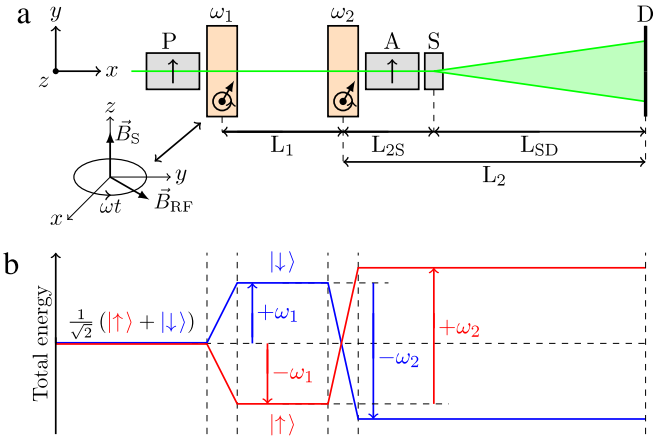

Fig. 1. (a) Sketch of a typical MIEZE setup. Along their flight path (from left to right), neutrons are first spin polarized (P) and manipulated by a sequence of two RFSF operated at field frequencies ω_1 and $\omega_2 \neq \omega_1$, respectively. Neutrons' spin are then analyzed (A), before being scattered by a sample (S) and detected by a time-resolved (ToF) detector (D). **Inset:** Superposition of a static field $\vec{B}_S$ and radio-frequency field $\vec{B}_{RF}$ as produced by the RFSF. $\vec{B}_{RF}$ is rotating in the plane perpendicular to $\vec{B}_S$ at an angular frequency $\omega = \gamma_n|\vec{B}_S|$, where $\gamma_n = 2\pi \cdot 2.916\,\mathrm{kHz\,G^{-1}}$ is the neutron gyromagnetic ratio. (b) Energy diagram of a neutron wave packet traveling across the MIEZE setup [5]. The initial wave function is split into two components with opposite spin, as quantified along the static field z-direction. This results in an energy difference $\Delta E = 2\hbar\omega_1$, which is reversed at the second flipper, yielding $\Delta E = 2\hbar(\omega_2 - \omega_1)$. The recombination of the neutron wave packet takes place at the detector where the spin phase is given by Eq. (1).

leading to a purely harmonic phase oscillation $\varphi_D(t_D) = \omega_M \cdot t_D$ at the detector position, even for a coarsely monochromated beam as prepared by a velocity selector. Placing a spin analyzer (A) between the second RFSF and the detector (D) transforms the *phase oscillation* into an *intensity modulation* $I_D(t_D) = I_0/2 \cdot \{1 + C \cdot \cos[\varphi_D(t_D)]\}$, which can be recorded using a time-resolved detector and where C is the signal contrast. If the neutron beam interacts with a sample (S), located between the analyzer and the detector, the time-dependent intensity will be modified by its dynamics. Indeed, energy transfers $\hbar\omega$ will induce a delay Δt_D in the neutron propagation time over the distance L_{SD}. Averaging this effect over all possible energy transfers yields a finite contrast

$$C \propto \langle \cos(\omega_M \Delta t_D) \rangle_{\hbar\omega} < 1 \tag{3}$$

with $\Delta t_D \equiv \dfrac{m_n L_{SD}}{h} \cdot \Delta\lambda = \dfrac{m_n^2}{2\pi h^2} L_{SD}\, \lambda^3\, \omega$,

where m_n is the neutron mass and h Planck's constant. Note that the definition of Δt_D in Eq. (3) is valid in the case of energy transfers which are centered around $\hbar\omega = 0$ and small with respect to the incoming neutron energy (quasi-elastic scattering). Assuming a ω-symmetric scattering function $S(q,\omega)$, Eq. (3) is equivalent to [20]

$$C \propto \frac{\int S(q,\omega)\cos(\omega\tau)\, d\omega}{\int S(q,\omega)\, d\omega} \equiv \frac{S(q,\tau)}{S(q,0)} \tag{4}$$

with $\tau = \dfrac{m_n^2}{2\pi h^2} \omega_M L_{SD} \lambda^3$.

In a MIEZE experiment, in full analogy with NSE spectroscopy, we thus have access to the intermediate scattering function, probing sample dynamics over time scales given by the instrumental Fourier time τ, which can reach several 100 ns. In contrast to usual neutron spectroscopy techniques (three-axis, time-of-flight or backscattering), this high-resolution is achieved without drastic loss of intensity since the measured signal does not depend on beam monochromaticity (Eqs. (1) and (2)). More interestingly, the main advantage of MIEZE is that the measurement is not affected by any depolarizing sample (spin incoherent scatterers [2], multi-domain ferromagnets [3], *etc.*) or environment (*e.g.* large magnetic fields [4]), as opposed to NSE.

On the downside, high-resolution can only be reached if no spurious spin phase shift is introduced in the problem, such a ones due to imperfections of the spin manipulation devices or to path length differences throughout the setup. Altogether, this results in an experimental contrast which takes the general form [21]

$$C(q,\tau) = \underbrace{\mathcal{R}_{coils}(\tau) \cdot \mathcal{R}_{sample}(q,\tau) \cdot \mathcal{R}_{det}(q,\tau)}_{\mathcal{R}} \cdot \frac{S(q,\tau)}{S(q,0)} \quad , \tag{5}$$

where the overall reduction factor $\mathcal{R}$ has to be properly quantified in order to correct data and deduce the intrinsic intermediate scattering function.

In practice, an analytical form of $\mathcal{R}_{coils}$ cannot be obtained since it involves fine details of the field distribution produced by the RFSF. However, the recent proposal to adopt a *longitudinal* (instead of the standard *transverse*) field geometry for the RFSF [22] allows keeping this term close to 1 in the experimental limit. This stems from a self-correction of RFSFs field inhomogeneities and a strongly suppressed field integral variation for divergent flight paths, notably reducing the current needed in correction (Fresnel) coils with respect to the NSE case (by a factor 3 at least) [23]. In what follows, we shall work under the assumption $\mathcal{R}_{coils} = 1$, keeping in mind that its actual value has to be measured before the experiment is performed.

The question of quantifying the reduction factors related to path length inhomogeneities due to sample size and detector thickness – $\mathcal{R}_{sample}$ and $\mathcal{R}_{det}$, respectively – has first been tackled numerically in [24]. In Refs. [21,25], the problem has been further specified by a combination of analytical calculations and Monte-Carlo simulations.

In this paper, we propose more general expressions for $\mathcal{R}_{sample}$ in the case of plate-like samples (parallelepipeds or disks), as usually encountered in soft-matter physics. We treat the case of a parallel incoming beam and the more realistic situation involving finite beam divergence (Section 2). In Section 3, we calculate the $\mathcal{R}_{det}$ term. Altogether, this allows defining the (q,τ)-range which is accessible under chosen experimental conditions and establishes MIEZE has an interesting counterpart of NSE (Section 4). Our findings call for the design of a MIEZE-SANS spectrometer, allowing to study the structure and ps-μs dynamics of any kind of large scale objects on a single instrument (Section 5).

2. Path length differences due to sample size and beam divergence

Let us consider a scattering configuration as depicted in Fig. 2a. In a first step, we shall treat the case of a parallel incoming beam where path length differences with respect to the optical axis read

$$\Delta L_2 = x - \frac{x \cdot \cos\theta_D + y \cdot \sin\theta_D}{\cos(2\theta - \theta_D)} \quad , \tag{6}$$

where x and y are the components of the vector $\vec{r}$ denoting the distance of an arbitrary scattering point to the center of the sample. This leads to a phase difference at the detector given by

$$\Delta\varphi_D = 2\pi \frac{\Delta L_2}{\Lambda} \quad , \tag{7}$$

where $\Lambda = 2\pi v/\omega_M$ is the distance traveled by a neutron of velocity v over one period $2\pi/\omega_M$ of the oscillating signal [21]. The contrast reduction factor is obtained by averaging $\cos(\Delta\varphi_D)$ over all possible neutron–sample interaction points. We end up with the following reduction factor:

$$\begin{aligned} \mathcal{R}_{sample} &\equiv \frac{\int_{-t/2}^{t/2}\int_{-w/2}^{w/2} \cos(\Delta\varphi_D)\, dy dx}{w \cdot t} \\ &= \mathrm{sinc}\left(\frac{\pi w}{\Lambda} \cdot \frac{\sin\theta_D}{\cos(2\theta - \theta_D)}\right) \\ &\times \mathrm{sinc}\left(\frac{\pi t}{\Lambda} \cdot \left[\frac{\cos\theta_D}{\cos(2\theta - \theta_D)} - 1\right]\right), \end{aligned} \tag{8}$$